Fluid Dynamics Research Group
Massachusetts Institute of Technology
Technical Report 58-4

SHOCK WAVE-LAMINAR BOUNDARY LAYER INTERACTION ON A CONVEX WALL

by

ISAAC GREBER

FOR THE

NATIONAL ADVISORY COMMITTEE

FOR

AERONAUTICS

CONTRACT NAw — 6462
NAw — 6507

JULY 1958

3

FLUID DYNAMICS RESEARCH GROUP

MASSACHUSETTS INSTITUTE OF TECHNOLOGY

TECHNICAL REPORT 58-4

SHOCK WAVE-LAMINAR BOUNDARY LAYER INTERACTION ON A CONVEX WALL

by

Isaac Greber

For the

National Advisory Committee
for
Aeronautics

CONTRACT NAw-6462
NAw-6507

July 1958

TABLE OF CONTENTS

Chapter No.		Page No.
...	Table of Contents	ii
...	Acknowledgements	iii
...	List of Figures	iv
...	List of Symbols	v
...	Summary	vii
I	Introduction	1
II	Experimental Apparatus and Technique	2
III	Pressure Distributions on Curved Plate	4
IV	Theoretical Model	5
...	Conclusions	15
...	References	16
...	Figures	17
...	Table 1	25
...	Table 2	26

ACKNOWLEDGEMENTS

The author wishes to thank Professor Leon Trilling and Mr. Saul Abarbanel for useful discussions, Mr. Kuo Chang Wang for helping to perform the experiments, and Mrs. Nancy Ramsdell for typing the manuscript.

List of Figures

Fig. 1	Cross-Section of Curved Plate
Fig. 2	Typical Pressure Distributions on Curved Plate
Fig. 3	Test of Parabolic Profile Near Wall
Fig. 4	Plateau Pressure Coefficients
Fig. 5	Skin Friction Coefficients
Fig. 6	Sketch of Flow Pattern at Incipient Separation
Fig. 7	Sketch of Flow Pattern with Separated Region
Fig. 8	Length of Plateau
Table I	Pressure Distributions on Curved Plate Without Shock Generator
Table II	Pressure Distributions on Curved Plate With Impinging Shock

List of Symbols

A	Constant of proportionality
h	Height above wall of line
K	Constant of proportionality
ℓ	Length of platèau
L	Distance from loading edge to end of plateau
$\mathcal{L}$	Length of plateau per unit driving pressure
M	Mach number
p	Pressure
p_d	Driving pressure to move separation print upstream
q	Dynamic pressure
r	Recovery factor
r_1	$\left(\frac{dp}{dx}\right)_0 / \left(\frac{dp}{dx}\right)_s$
r_2	$\frac{\ell \left(\partial p/\partial x\right)_0}{p_{pl.} - p_0}$
u	Component of velocity parallel to plate
v	Component of velocity normal to plate
x	Length parallel to plate measured from leading edge of plate
y	Length normal to plate
α	Flow deflection angle
β	$\sqrt{M^2 - 1}$
γ	Specific heat ratio
ε	Effective height which the undisturbed boundary layer is lifted from the wall
ε_1	Height at which inner and outer profiles are joined
μ	Dynamic viscosity coefficient
ρ	Density
τ	Sheer stress $= \mu \frac{\partial u}{\partial y}$

Subscripts

0	Conditions at the beginning of interaction
∞	Conditions in the free stream upstream of the body
B	Conditions on the surface in the absence of interaction
f	Conditions in the "final" state just after the interaction is complete
f.p.	Flat plate conditions
pl.	Plateau
r	Reattachment point
s	Separation point
sh	Shock
w	Wall
ε	Conditions at the height ε

Summary

The results of some experimental and theoretical studies of the interaction of oblique shock waves with laminar boundary layers on a curved surface are presented. The theoretical work extends a flat plate model previously derived, to include the effects of surface curvature on the pressure levels characteristic of separation and on the length of the separated region. Pressure measurements on a curved surface bear out the prediction of the pressure in the constant pressure separated region. The measurements of length of separated region are not conclusive due to insufficient data for long separated regions.

Chapter I

Introduction

In Ref. 1 experimental results were presented and a theoretical model derived for the interaction of oblique shock waves with laminar boundary layers on a flat surface. The present work constitutes an extension of the previous work to include the effects of surface curvature.

The experimental part of this work consists primarily of pressure measurements made during shock wave-boundary layer interaction. Some boundary layer measurements were made in the absence of interaction in order to check the boundary layer calculations.

The theoretical work extends the simple model proposed in Ref. 1. It is found that convex surface curvature decreases all the pressure levels characteristic of separation, but increases the shock strength needed to separate a laminar boundary layer. For a given "driving pressure" (defined later), convex surface curvature decreases the length of the constant pressure region.

The experiments verify the theoretical prediction of the pressure in the constant pressure separated region. There are insufficient data for long separated regions to verify properly the prediction of length of separated region.

Chapter II

Experimental Apparatus and Technique

Wind Tunnel

The experiments were performed in the 8 in. by 8 in. continuous flow supersonic wind tunnel in the Gas Turbine Laboratory of the Massachusetts Institute of Technology. This tunnel has a fixed M = 2 nozzle with an upward flow direction. A standard Schlieren optical system is available for observing and photgraphing the flow. The tunnel can be operated at stagnation pressures ranging approximately from 3 to 15 psi absolute, using a steam ejector system for evacuation to sub-atmospheric levels. This is the same tunnel and auxiliary equipment which was used in the work described in Ref. 1.

Curved Plate

A cross-section of the curved plate is shown in Fig. 1. The plate fully spans the test section of the tunnel. The plate has static pressure orifices drilled at one-tenth of an inch spacing to measure streamwise pressure distribution. Two rows of static pressure orifices are drilled across the plate to check two-dimensionality of the flow. Pressures were read either on mercury or Meriam fluid (specific gravity 2.95) manometers, depending on the pressure level. Two thermocouples are imbedded in the plate surface, and their readings were measured by means of a standard potentiometer. Stagnation pressure and temperature were measured similarly, with orifice and thermocouple installed in the settling chamber.

Shock Generator

The adjustable angle shock generators developed by Barry, Shapiro, and Neumann (Ref. 2) for the tunnel were used without changes.

Velocity Profile and Skin Friction Measurement

The total head in the boundary layer was measured by a small slit mouth tube which could be moved by controls outside of the tunnel. The tube height is about 0.004 inches and the opening is about 0.001 inches. In taking surveys normal to the plate, the tube location was observed through a telescope which moves on a fine screw thread; the telescope's location was measured with a micrometer fixed to the telescope mount.

The same tube was also used to measure local skin friction by taking measurements with the tube resting on the plate. The tube had previously been so calibrated as a skin friction meter (Ref. 3).

Range of Measurements

The experiments were performed at several different stagnation pressure (i.e. Reynolds number) levels, and with varying shock strengths. The shock strengths ranged from those small enough not to cause separation to cases involving extended upstream influence. For the shock interaction experiments, the Reynolds number based on distance from leading edge to beginning of interaction ranged approximately from 1.8×10^5 to 5.7×10^5. With no external shock, separation was caused by downstream compressive turning; in these measurements, the corresponding Reynolds number range was 1.6×10^5 to 8.7×10^5. In addition, there was a maverick run in which separation was caused apparently by downstream chocking; the Reynolds number was $.47 \times 10^5$. The total Reynolds number range based on distance from leading edge to beginning of interaction therefore was $.47 \times 10^5$ to 8.7×10^5

Chapter III

Pressure Distributions on Curved Plate

Typical streamwise pressure distributions are shown in Fig. 2. Curve A is a pressure distribution with no shock generator. The plateau is due to separation caused by the compressive turning of the flow downstream of the convex surface. Curve B shows a distribution for a shock not strong enough to cause separation. Downstream of the shock the negative gradient due to the convex curvature of the surface is again apparent, as is the separation plateau caused by downstream compressive turning. Curves C and D show distributions with shock-induced separation. After reattachment the negative pressure gradient manifests itself, but downstream separation due to compressive turning does not occur. The probable reason is that the reattached boundary layer is turbulent.

All of the measured pressure distributions are given in Tables I and II. The qualitative behavior is the same as that described above.

Chapter IV

Theoretical Model

Pressure Rise to Separation

As in Ref. 1, the pressure rise to separation is found by dividing the boundary layer into a slow flow near the wall and an essentially undisturbed outer profile, and saying that the pressure rise is due to the apparent geometric lifting of the undisturbed boundary layer. A sketch of this model is shown below:

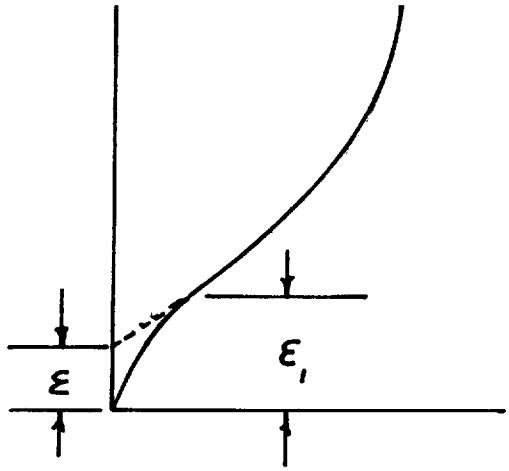

If the sublayer is assumed to have negligible momentum, then the integral of the momentum equation from the wall to ε is:

$$\varepsilon \frac{dp}{dx} = \tau_\varepsilon - \tau_w \qquad (1)$$

Taking the pressure rise to be due to the growth of ε and assuming small perturbations, the pressure rise is related to the growth of the sublayer by

$$\frac{p - p_B}{q_\infty} = \frac{2}{\beta_\infty} \frac{d\varepsilon}{dx} \qquad (2)$$

Eliminating ε between (1) and (2) leads to

$$\frac{\beta_\infty}{2}\frac{dp}{dx}\int_{x_0}^{x}\frac{p-p_B}{q_\infty}dx = \tau_\varepsilon - \tau_w \qquad (3)$$

Taking constant body pressure gradient and constant $\frac{dp}{dx}$ (this is true except for a small region in which $p-p_B$ is small), and evaluating (3) at the separation point where $\tau_w = 0$, there results

$$\frac{\beta_\infty}{4}\left(\frac{p_s-p_0}{q_\infty}\right)^2\left[1-\frac{p_B-p_0}{p_s-p_0}\right] = \frac{\tau_{\varepsilon_s}}{q_\infty} \qquad (4)$$

For constant pressure gradients, this can be written

$$\frac{\beta_\infty}{4}\left(\frac{p_s-p_0}{q_\infty}\right)^2\left[1-\frac{(dp/dx)_B}{(dp/dx)_s}\right] = \frac{\tau_{\varepsilon_s}}{q_\infty} \qquad (5)$$

τ_{ε_s} is found by making the velocity and sheer stress continuous at ε_1 . Consistent with (1):

$$u(\varepsilon_1) = \frac{1}{\mu_w}\left[\tau_w\varepsilon_1 + \frac{1}{2}\frac{dp}{dx}\varepsilon_1^2\right] \qquad (6)$$

$$\tau(\varepsilon_1) = \tau_w + \frac{dp}{dx}\varepsilon_1 \qquad (7)$$

From the undisturbed profile:

$$u(\varepsilon_1) = \frac{1}{\mu_{w_0}}\left[\tau_{w_0}(\varepsilon_1-\varepsilon) + \frac{1}{2}\left(\frac{dp}{dx}\right)_0(\varepsilon_1-\varepsilon)^2\right] \qquad (8)$$

$$\tau(\varepsilon_1) = \tau_{w_0} + \left(\frac{dp}{dx}\right)_0(\varepsilon_1-\varepsilon) \qquad (9)$$

Setting $\tau_w = 0$, solving for ε , setting $\frac{\mu_{w_0}}{\mu_w} = 1$ and finding τ_ε from (1) gives:

$$\frac{\tau_{\varepsilon_s}}{\tau_{w_0}} = \left[1+\sqrt{1-\frac{(dp/dx)_0}{(dp/dx)_s}}\right]^{-1} \qquad (10)$$

Putting (10) into (5) gives for the separation pressure rise

$$\frac{p_s - p_0}{q_\infty} = 2\sqrt{\frac{\tau_0/q_\infty}{\beta_\infty}}\left[\left(1-\frac{(dp/dx)_B}{(dp/dx)_s}\right)\left(1+\sqrt{1-\frac{(dp/dx)_B}{(dp/dx)_s}}\right)\right]^{-1/2} \quad (11)$$

For small $\frac{(dp/dx)_0}{(dp/dx)_s}$ and $\frac{(dp/dx)_B}{(dp/dx)_s}$, binomial expansion gives:

$$\frac{p_s - p_0}{q_\infty} \approx \sqrt{\frac{2\tau_0/q_\infty}{\beta_\infty}}\left[1+\frac{1}{2}\frac{(dp/dx)_B}{(dp/dx)_{s0}}\left(1+\frac{1}{4}\frac{(dp/dx)_0}{(dp/dx)_B}\right)\right] \quad (12)$$

where $(dp/dx)_{s0}$ is the pressure gradient which would exist at separation in the absence of body curvature. If $(dp/dx)_B = (dp/dx)_0 = 0$, (11) or (12) reduces, of course, to the result given in Ref. 1. Except near rapid changes in body curvature, $(dp/dx)_0 = (dp/dx)_B$ Equation (12) indicates that the direct effect of body curvature, $(dp/dx)_B$ is more important in altering the separation pressure rise than is the boundary layer curvature due to initial pressure gradient $(dp/dx)_0$. Furthermore, for negative pressure gradients the parabolic profile given by Equation (8) is not a good approximation and overestimates the effect of pressure gradient. Comparison of the parabolic profile with a measured profile is shown in Fig. 3, where the inadequacy of the parabolic approximation is apparent. Since the parabolic profile overestimates the importance of initial pressure gradient, and since even with this overestimate initial pressure gradient is found to be much less important than the geometrical effect of body curvature, initial pressure gradient will be neglected. The initial boundary layer then is described only by its shear stress at the wall, and the separation pressure rise is given by

$$\frac{p_s - p_0}{q_\infty} = \sqrt{\frac{2\tau_0/q_\infty}{\beta_\infty}}\left[1-\frac{(dp/dx)_B}{(dp/dx)_s}\right]^{-1/2} \quad (13)$$

Negative pressure gradient is seen to reduce the pressure rise to separation. As in Ref. 1, the pressure rise to the plateau is taken to be a constant multiple of the pressure rise to separation:

$$\frac{p_{pl}-p_o}{q_\infty} = A\sqrt{\frac{2\theta_o/q_\infty}{\beta_\infty}}\left[1-\frac{(dp/dx)_o}{(dp/dx)_s}\right]^{-1/2} \qquad (14)$$

A correlation of the experimental plateau pressure rises according to equation (14) is shown in Fig. 4. Skin friction was computed by Hill's method (Ref. 4), which is a reduction of the momentum integral to quadrature through an assumption of the flat plate relation between wall shear and momentum thickness Reynolds number. The calculated skin friction agrees reasonably within the scatter of the measured values (Fig. 5), and was used rather than trying to fit an average curve through the experimental points. From Fig. 4 the plateau pressure rise is seen to be well correlated by Equation (14). The same constant "A" correlates plateau pressures caused by shock induced separation on the curved and flat plates (flat plate data from Ref. 1), and due to separation caused by downstream compressive turning. With "A" = 1.54, one finally has:

$$\frac{p_{pl}-p_o}{q_\infty} = 2.17\sqrt{\frac{\theta_o/q_\infty}{\beta_\infty}}\left[1-\frac{(dp/dx)_o}{(dp/dx)_s}\right]^{-1/2} \qquad (15)$$

Pressure Rise for Incipient Separation

If the wall shear is just brought to zero at one point, with no separated region developing, then the physical picture is that the shock reaches the boundary layer at the separation point and reflects as an expansion wave which cancels the pressure rise due to the shock, so that the pressure is continuous in the subsonic flow. The flow then turns parallel to the wall at a rate dictated by the thinning of the boundary layer. A sketch of this model is shown in Fig. 6.

The pressure rise from the reattachment point to the final value can be analyzed by a sublayer model in a similar manner to the analysis of the pressure rise to separation. Perturbing about the final state, one writes quite analogously to equation (13):

$$\frac{p_f - p_r}{q_f} = \sqrt{\frac{2\tau_f/\rho_f}{\beta_f}} \left[1 - \frac{(dp/dx)_B}{(dp/dx)_r} \right]^{-1/2} \qquad (16)$$

where the subscript "r" denotes reattachment and the subscript "f" denotes the final state. For incipient separation the separation and the reattachment point are the same, and the pressure rise from initial to final state is given by the sum of (13) and (16):

$$(p_f - p_0)_{INCIP.} = \sqrt{\frac{2\tau_\infty/\rho_\infty}{\beta_\infty}} \left[1 - \frac{(dp/dx)_B}{(dp/dx)_s} \right]^{-1/2} q_\infty + \sqrt{\frac{2\tau_f/\rho_f}{\beta_f}} \left[1 - \frac{(dp/dx)_B}{(dp/dx)_r} \right]^{-1/2} q_f \qquad (17)$$

Assuming that at the separation point the pressure gradient and the shear stress at the effective lifted height are continous, and taking the incident shock to be sufficiently weak so that the stagnation pressure change can be neglected, then one derives from (17)

$$\left(\frac{p_f - p_0}{q_\infty} \right)_{INCIP.} = 2\sqrt{\frac{2\tau_\infty/\rho_\infty}{\beta_\infty}} \left[1 - \frac{(dp/dx)_B}{(dp/dx)_s} \right]^{-1/2} \qquad (18)$$

From this point of view, the shock acts merely as a device to turn the flow, without changing its entropy. To calculate the strength of the required shock, its turning angle can be calculated by equating the actual turning of the flow during the interaction process to the change in angle of the surface. Assuming a weak incident shock, so that the incident shock and the reflected expansion each turns the flow through an angle α, the angle equation is

$$\frac{\beta_\infty}{2}\left(\frac{p_{t_B} - p_0}{q_\infty} \right) = \frac{\beta_\infty}{2}\left(\frac{p_s - p_0}{q_\infty} \right) + \frac{\beta_f}{2}\left(\frac{p_f - p_s}{q_f} \right) - 2\alpha \qquad (19)$$

or approximately

$$\alpha = \frac{\beta}{4}\left[\frac{p_t - p_0}{q_\infty} - \frac{p_{t_B} - p_0}{q_\infty}\right] \qquad (20)$$

Therefore

$$\left(\frac{p_{sh.} - p_s}{q_\infty}\right)_{INCIP.} = \frac{1}{2}\frac{p_t - p_0}{q_\infty}\left[1 - \frac{(dp/dx)_B}{(dp/dx)_s}\right] \qquad (21)$$

Using (18), Equation (21) leads to:

$$\left(\frac{p_{sh.} - p_s}{q_\infty}\right)_{INCIP.} = \sqrt{\frac{2\tau_0/q_\infty}{\beta_\infty}}\sqrt{1 - \frac{(dp/dx)_B}{(dp/dx)_s}} \qquad (22)$$

Equation (19) is a local equation, and hence formally Equation (22) gives the local strength of the incident shock in the vicinity of the shock impingement point. However, since the weak shock assumption has been introduced, the same expression could have been derived by considering the overall reflection of a shock wave from the wall. Therefore, the free stream strength of the shock is

$$\left(\frac{p_{sh.} - p_\infty}{q_\infty}\right)_{INCIP.} = \sqrt{\frac{2\tau_0/q_\infty}{\beta_\infty}}\sqrt{1 - \frac{(dp/dx)_B}{(dp/dx)_s}} \qquad (23)$$

Thus, for given Mach number and skin friction coefficient, convex curvature ($(\frac{dp}{dx})_B < 0$) increases the shock strength needed to separate a boundary layer. However, the surface pressure rise is decreased, in accordance with equation (18).

The incipient separation pressure formulas cannot be tested directly from the pressure measurements. About all that can be said is that clearly higher pressure rises than those given by Equation (18) are needed to cause a pressure plateau.

Length of the Separated Region

If the shock strength is greater than that required for incipient separation, the separation point moves upstream of the shock impingement point. If the separation point moves sufficiently far upstream, a constant pressure "plateau" occurs. In principle, the regions upstream and downstream of the shock impingement point can be computed from a model of an outer

flow which is locally altered by the thickening and thinning of the boundary layer. The complete interaction pattern is determined by choosing combinations of separating conditions, reattaching conditions and shock strengths so that the flow is self-consistent. The limiting case for incipient separation has already been given. Further calculations of this sort with non-zero length of separated region have not yet been done. Instead what is given below is an estimate of the length upstream of the shock impingement point when a long plateau exists. The calculation follows that of Ref. 1, and is intended primarily to display the effect of surface curvature.

The basic argument is that when the flow is completely separated, the height of the separated region depends on the mass of fluid forced into the backflow by the overpressure left available from the main shock after subtracting the pressure rise to the plateau plus the pressure rise for the reattachment process.

A sketch of the physical model is shown in Fig. 7. All of the fluid which is reversed must come from above the line $u = o$. One examines the integral of the boundary layer momentum equation

$$\int \left[\rho u \frac{\partial u}{\partial x} + \rho v \frac{\partial u}{\partial y} + \frac{dp}{dx} \right] dx = \int \frac{\partial \tau}{\partial y} dx \qquad (24)$$

along the line $u = o$ from the shock impingement point to the reattachment point. Neglecting $\int \frac{\partial \tau}{\partial y} dx$, one writes

$$\Delta p_d \approx - \int \rho v \frac{\partial u}{\partial y} dx \qquad (25)$$

where Δp_d is the driving pressure for the reverse flow. Taking averages

$$\Delta p_d \approx - \rho_w \bar{v} \frac{\bar{\tau}}{\mu_w} \Delta x \qquad (26)$$

By continuity, $\rho_w \bar{v} \Delta x = \rho_w \bar{u} h_{MAX.}$ where h

is the height of the line $u=o$, and $\bar{u}$ is the average velocity below $u=o$. Therefore

$$\Delta p_d \frac{\mu_w}{\tau} = -\rho_w \bar{u} h_{MAX.} \tag{27}$$

A momentum balance below $u=o$ at $h_{MAX.}$ gives approximately

$$\rho_w \bar{u}^2 \frac{dh}{dx} = \tau_{u=o} - \tau_w \tag{28}$$

Eliminating $\bar{u}$ between (27) and (28) gives

$$(\Delta p_d)^2 \frac{dh}{dx} = \rho_w \left(\frac{\tau}{\mu_w}\right)^2 (h_{MAX})^2 (\tau_{u=o} - \tau_w) \tag{29}$$

Now,

$$\frac{dh}{dx} = \frac{\beta_\infty}{2}\left[\frac{p_{gl} - p_B}{q_\infty}\right] = \frac{\beta_\infty}{2}\left[\frac{p_{gl} - p_o}{q_\infty}\right]\left[1 - \frac{(dp/dx)_B}{(dp/dx)_s} - \frac{(x - x_{gl})(dp/dx)_B}{p_{gl} - p_o}\right] \tag{30}$$

and

$$h = h_{gl.} + \int_{x_{gl}}^{x} \frac{dh}{dx} dx = \frac{\beta_\infty}{2}(x - x_{gl})\left[\frac{p_{gl} - p_{B_{gl}}}{q_\infty} - \frac{p_B - p_{B_{gl}}}{2 q_\infty}\right] \tag{31}$$

Neglecting $h_{gl.}$ one gets:

$$\frac{h_{MAX.}}{l} = \frac{\beta_\infty}{2} \frac{p_{gl} - p_o}{q_\infty}\left[1 - \frac{(dp/dx)_B}{(dp/dx)_s} - \frac{l}{2}\frac{(dp/dx)_B}{p_{gl} - p_o}\right] \tag{32}$$

Putting (30) and (32) into (29) gives:

$$(\Delta p_d)^2\left[1 - \frac{(dp/dx)_B}{(dp/dx)_s} - \frac{l\,(dp/dx)_B}{p_{gl} - p_o}\right] = \rho_w \left(\frac{\tau}{\mu_w}\right)^2 \frac{\beta_\infty}{2}\left[1 - \frac{(dp/dx)_B}{(dp/dx)_s} - \frac{l}{2}\frac{(dp/dx)_B}{p_{gl} - p_o}\right]^2 \frac{p_{gl} - p_o}{q_\infty} l^2 (\tau_{u=o} - \tau_w) \tag{33}$$

Now,

$$\frac{p_{gl} - p_o}{q_\infty} = A\sqrt{\frac{2\tau_o/\rho_\infty}{\beta_\infty}}\left[1 - \frac{(dp/dx)_B}{(dp/dx)_s}\right]^{-1/2} \tag{14}$$

Putting (14) into (33), and calculating the effect of surface curvature for given initial conditions and shear stress,

one gets that

$$\frac{\ell/\Delta p_d}{(\ell/\Delta p_d)_{f.p.}} = \frac{\left[1-\frac{(dp/dx)_B}{(dp/dx)_s}-\frac{\ell\,(dp/dx)_B}{p_{pl}-p_0}\right]^{1/2}\left[1-\frac{(dp/dx)_B}{(dp/dx)_s}\right]^{1/4}}{1-\frac{(dp/dx)_B}{(dp/dx)_s}-\frac{\ell}{2}\frac{(dp/dx)_B}{p_{pl}-p_0}} \qquad (34)$$

where the subscript "f.p." denotes the flat plate value.

Define:

$$\frac{(dp/dx)_B}{(dp/dx)_s} \equiv r_1 \;;\; \frac{\ell\,(dp/dx)_B}{p_{pl}-p_0} \equiv r_2 \;;\; \frac{\ell}{\Delta p_d} \equiv \mathcal{L} \qquad (35)$$

therefore

$$\frac{\mathcal{L}}{\mathcal{L}_{f.p.}} = \frac{(1-r_1-r_2)^{1/2}(1-r_1)^{1/4}}{1-r_1-\frac{1}{2}r_2} \qquad (36)$$

Equation (36) can be rewritten

$$\frac{\mathcal{L}}{\mathcal{L}_{f.p.}} = \frac{\sqrt{1-r_2}}{1-r_2/2}\,\frac{\sqrt{1-\frac{r_1}{1-r_2}}}{1-\frac{r_1}{1-r_2/2}}\,(1-r_1)^{1/4} \qquad (37)$$

For convex curvature, r_1 and r_2 are negative; the first two factors on the right hand side of (37) are less than unity and the third is greater than unity. In general, $\mathcal{L}/\mathcal{L}_{f.p.} < 1$ For long plateaus, $\frac{r_1}{1-r_2} << 1$ and the second factor on the right hand side of (37) is nearly unity, but the first factor is small enough to ensure $\mathcal{L}/\mathcal{L}_{f.p.} < 1$. For moderate plateaus, the second factor is sufficiently small so that the last two factors give a product less than unity.

For the experiments reported herein, the lengths of separated region are too small to display an important effect of surface curvature. With the experimental r_1 and r_2, $\mathcal{L}/\mathcal{L}_{f.p.}$ ranges approximately from .82 to .95.

An attempt was made to compare the present results with the flat plate results of Ref. 1. If in Equation (33) all the shear stresses are taken to be proportional to each other, then one can write the approximate relation.

$$\frac{\ell}{L} = K\,\frac{\mathcal{L}}{\mathcal{L}_{f.p.}}\left[1+\frac{\gamma-1}{2}r M_{ab}^2\right]^{3/2}\beta_{ab}^{-1/4}\left(\frac{r_0}{\rho_{ab}}\right)^{1/4}\frac{\Delta p_d}{q_{ab}} \qquad (38)$$

In Ref. 1 the driving pressure was taken to be the difference between the pressure rise from the beginning of interaction to the final state and the pressure rise required for incipient separation. It was found that for the longer plateaus $K = 2.53$, and Equation (38) has an additive constant .097. Thus one expects

$$\frac{\ell}{L} = 2.53 \frac{I}{I_{s.p.}} \left[1 + \frac{\gamma-1}{2} r M_\infty^2\right]^{3/2} \beta_\infty^{-1/4} \left(\frac{\tau_0}{q_\infty}\right)^{1/4} \frac{\Delta p_d}{q_\infty} + .097 \qquad (39)$$

The driving pressure is given by:

$$\frac{\Delta p_d}{q_\infty} = \frac{p_f - p_0}{q_\infty} - 1.21 \frac{p_{pl} - p_0}{q_\infty} \qquad (40)$$

In Fig. 8 the present curved plate data and the flat plate data of Ref. 1 are plotted according to Equation (39). It is clear that for the shorter plateaus  something missing as expected. However, there is insufficient long plateau data to determine whether equation (39) correlates the long plateaus.

Conclusions

The effect of surface curvature on the interaction of shock waves with laminar boundary layers has been investigated. An extension of a simple mathematical model previously derived on the basis of flat plate measurements shows that convex surface curvature reduces the pressure rises characteristic of separation, increases the strength of the incident shock wave required to separate a laminar boundary layer, and decreases the length of the constant pressure separated region for a given driving pressure. The decrease of the characteristic separation pressures is equivalent to a superposition of the pressure fields due to the body alone and due to the boundary layer. For the shorter plateaus the effect of convex surface curvature on the plateau length is less important than its effect on the characteristic separation pressures; the effect on plateau length becomes stronger for the longer plateaus.

The pressure measurements confirm the predicted effect of convex surface curvature on the pressure in the constant pressure separated region. There is insufficient long plateau data to verify properly the theoretical prediction of the length of the plateau.

References

1. Hakkinen, R. J., Greber, I., Trilling, L., Abarbanel, S. S., The Interaction of an Oblique Shock Wave with a Laminar Boundary Layer, Fluid Dynamics Research Group, M. I. T., Tech. Report 57-1, May 1, 1957.

2. Barry, F. W., Shapiro, A. H., Neumann, E. P., The Interaction of Shock Waves with Boundary Layers on a Flat Surface, M. I. T. Meteor Report 52, 1950.

3. Abarbanel, S. S., Hakkinen, R. J., Trilling, L., The Use of Stanton Tube for Skin Friction Measurements, Fluid Dynamics Research Group, M. I. T., Tech. Report 57-3, July 1, 1957.

4. Hill, J. A. F., Approximate Methods for Calculating the Development of Boundary Layers on Surfaces with Arbitrary Distributions of Velocity and Surface Temperature, Chapter IV of "Notes for a Special Summer Program in Aerodynamic Heating of Aircraft Structures in High Speed Flight," Department of Aeronautical Engineering, M. I. T., June 1956.

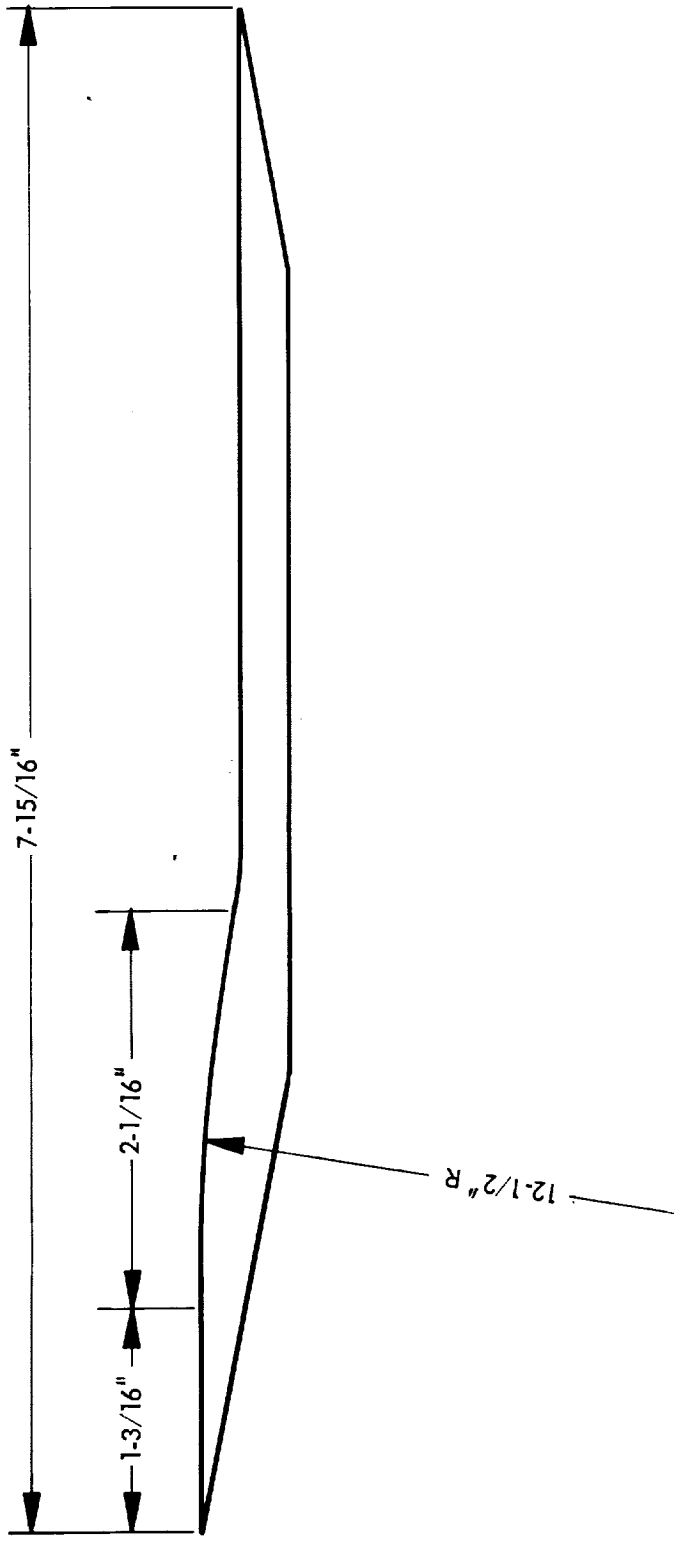

Fig. 1. Cross-section of curved plate.

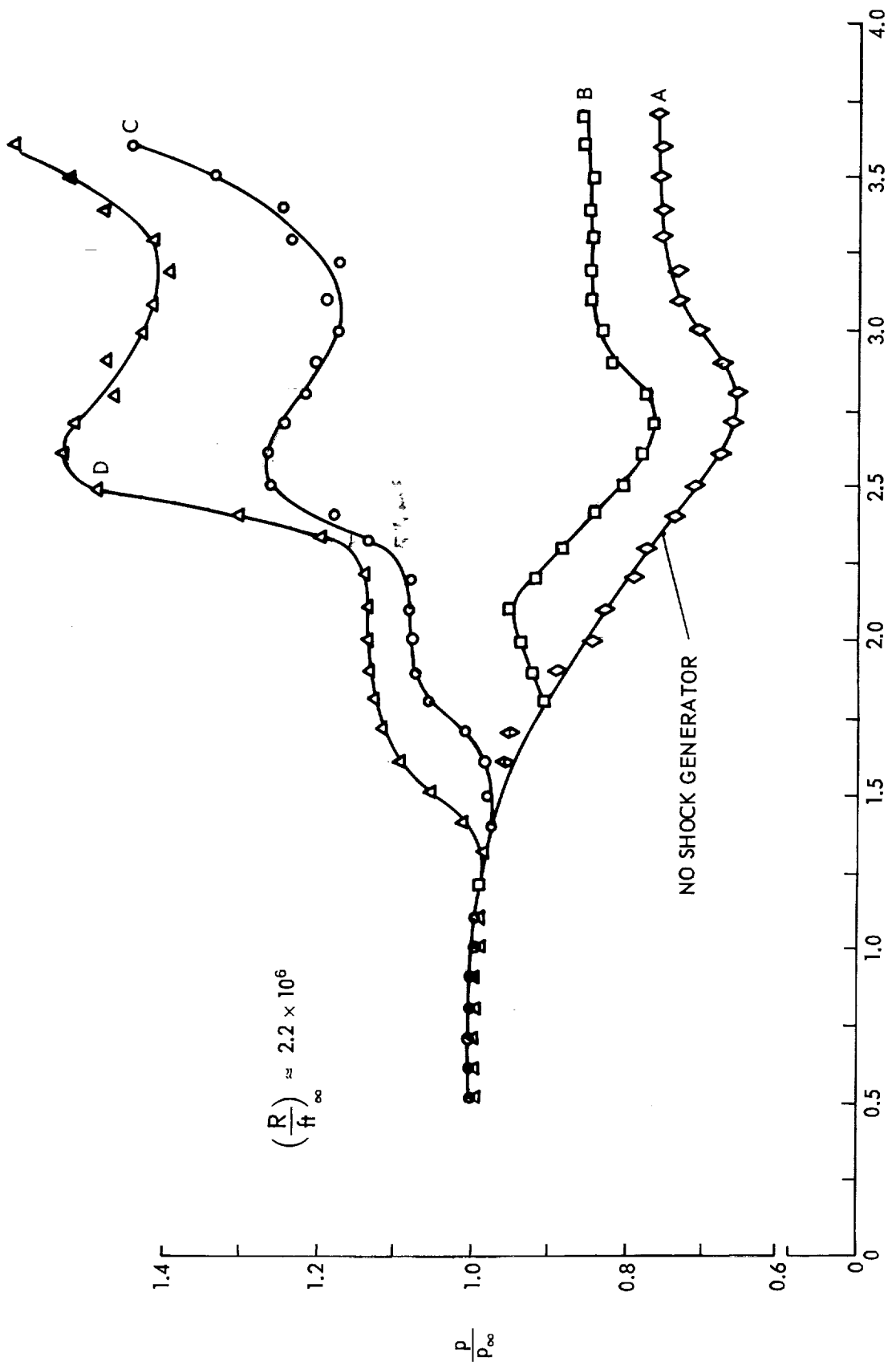

Fig. 2. Typical pressure distributions on curved plate.

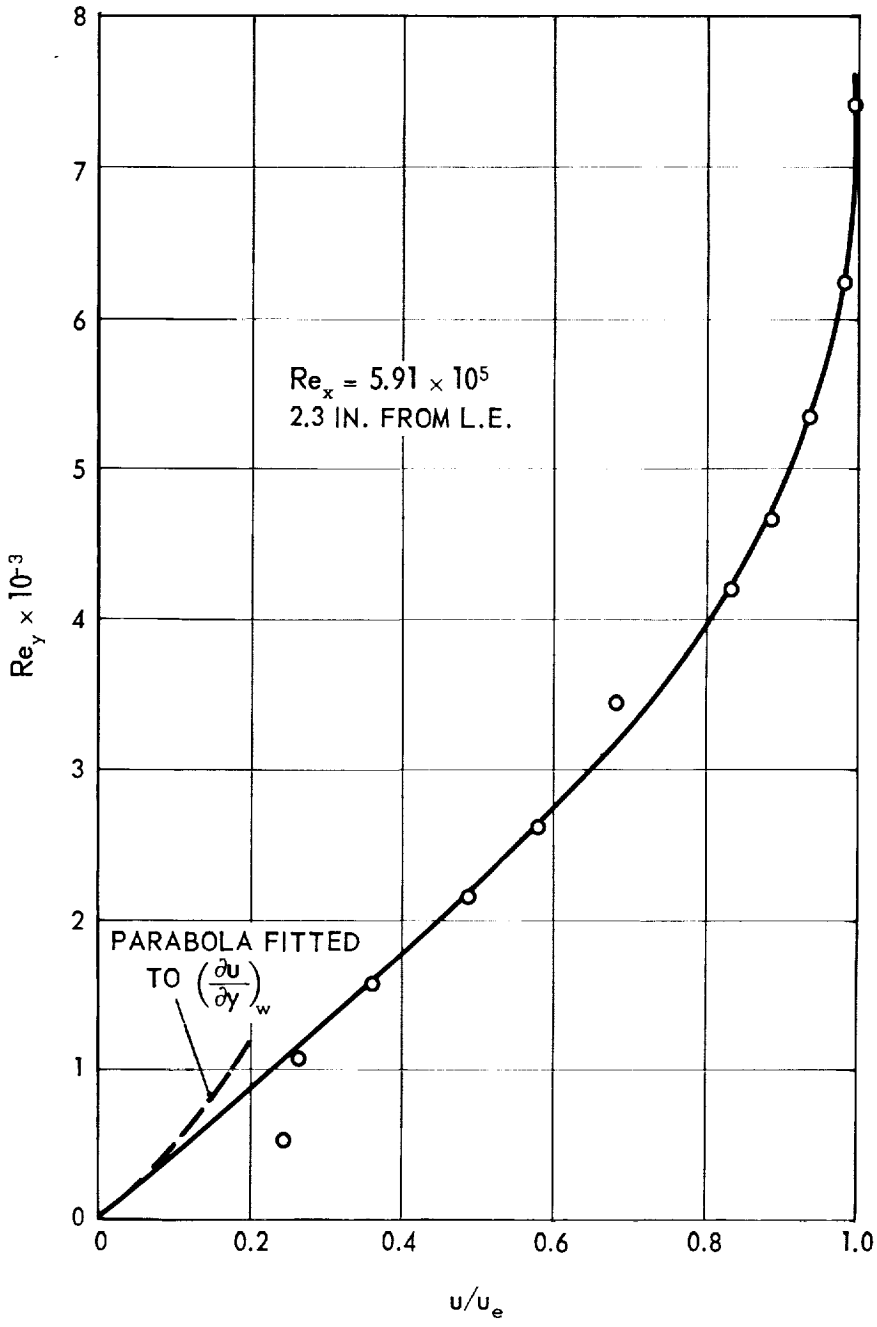

Fig. 3. Test of parabolic profile near wall.

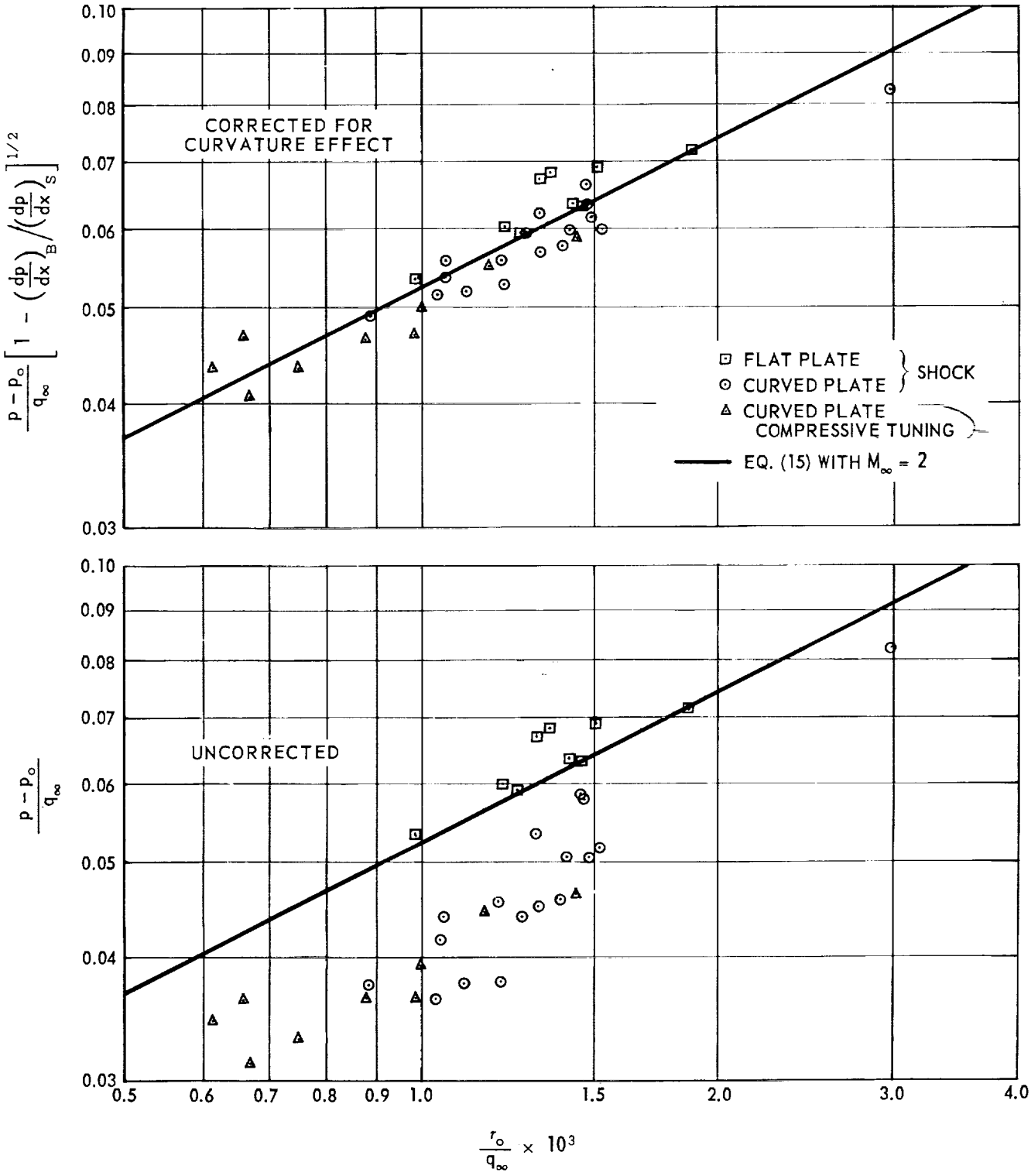

Fig. 4. Plateau pressure coefficients.

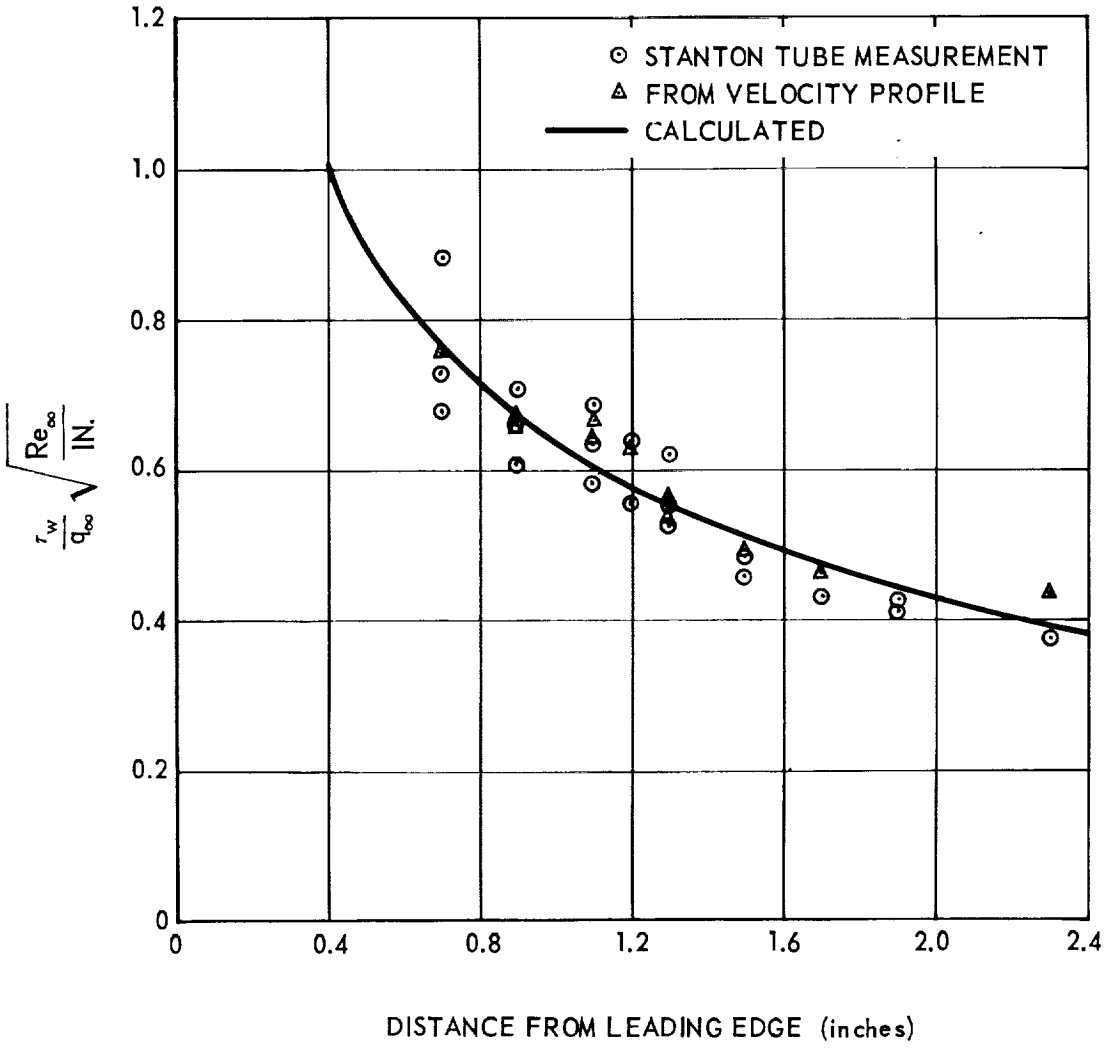

Fig. 5. Skin friction coefficients.

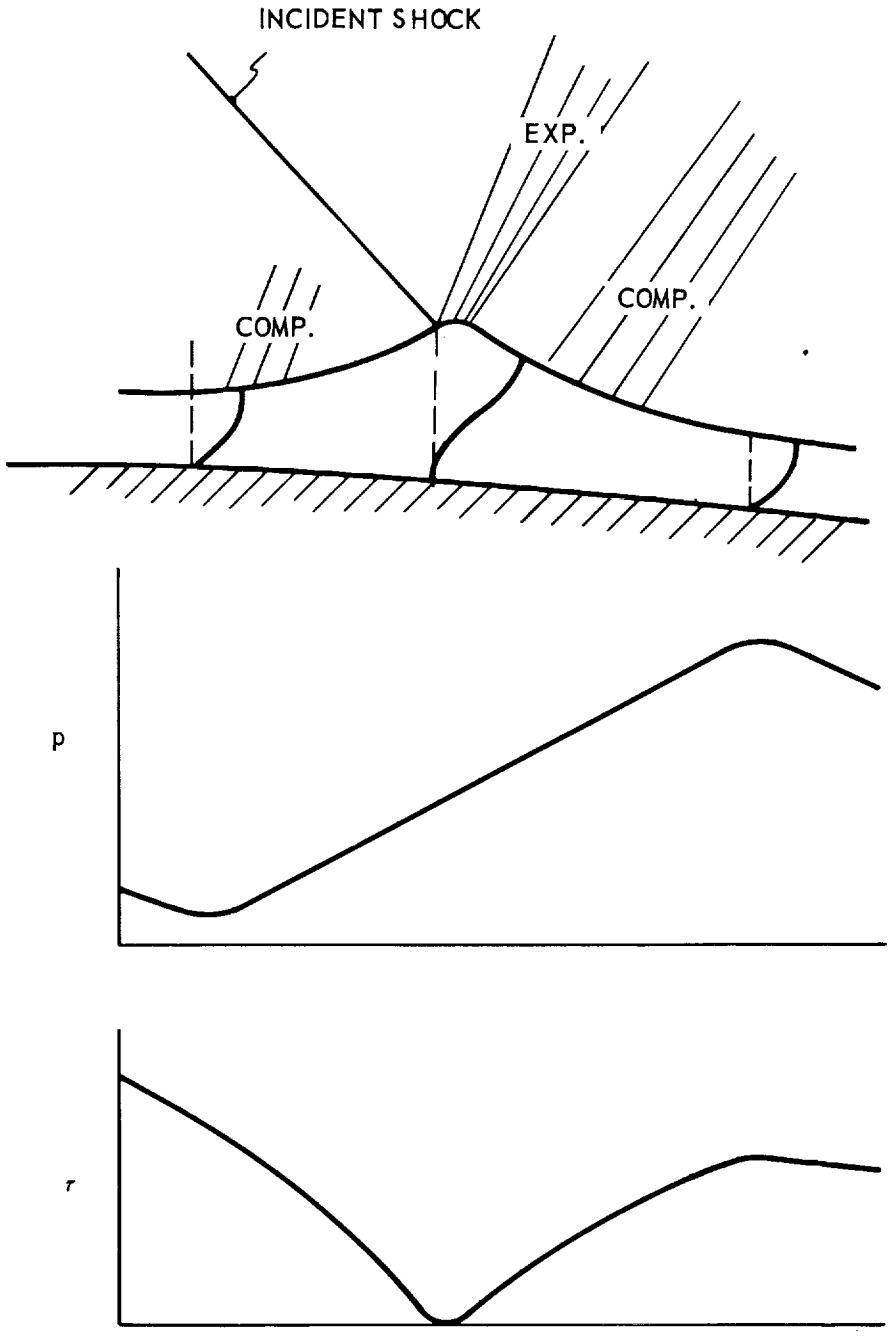

Fig. 6. Sketch of flow pattern at incipient separation.

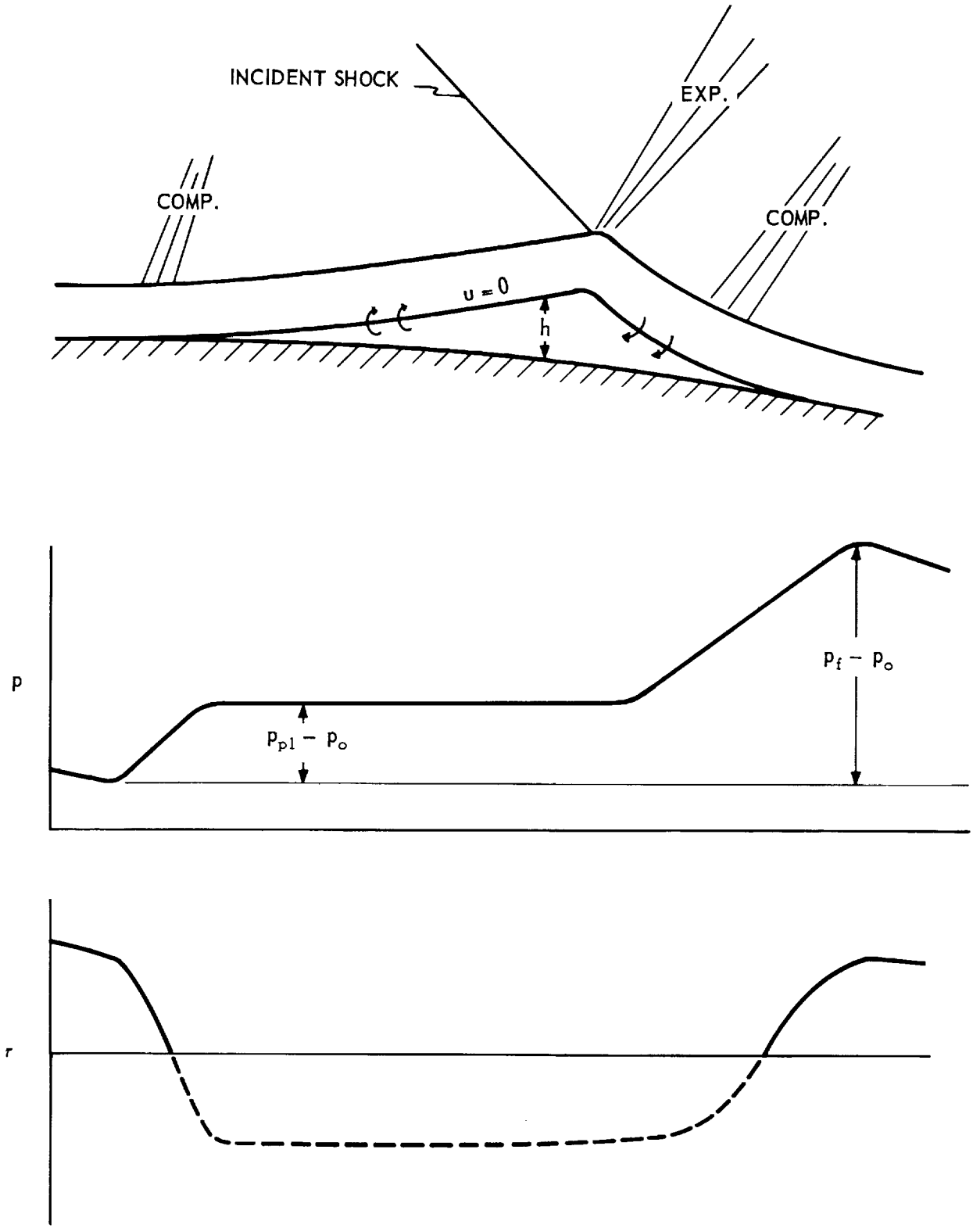

Fig. 7. Sketch of flow pattern with separated region.

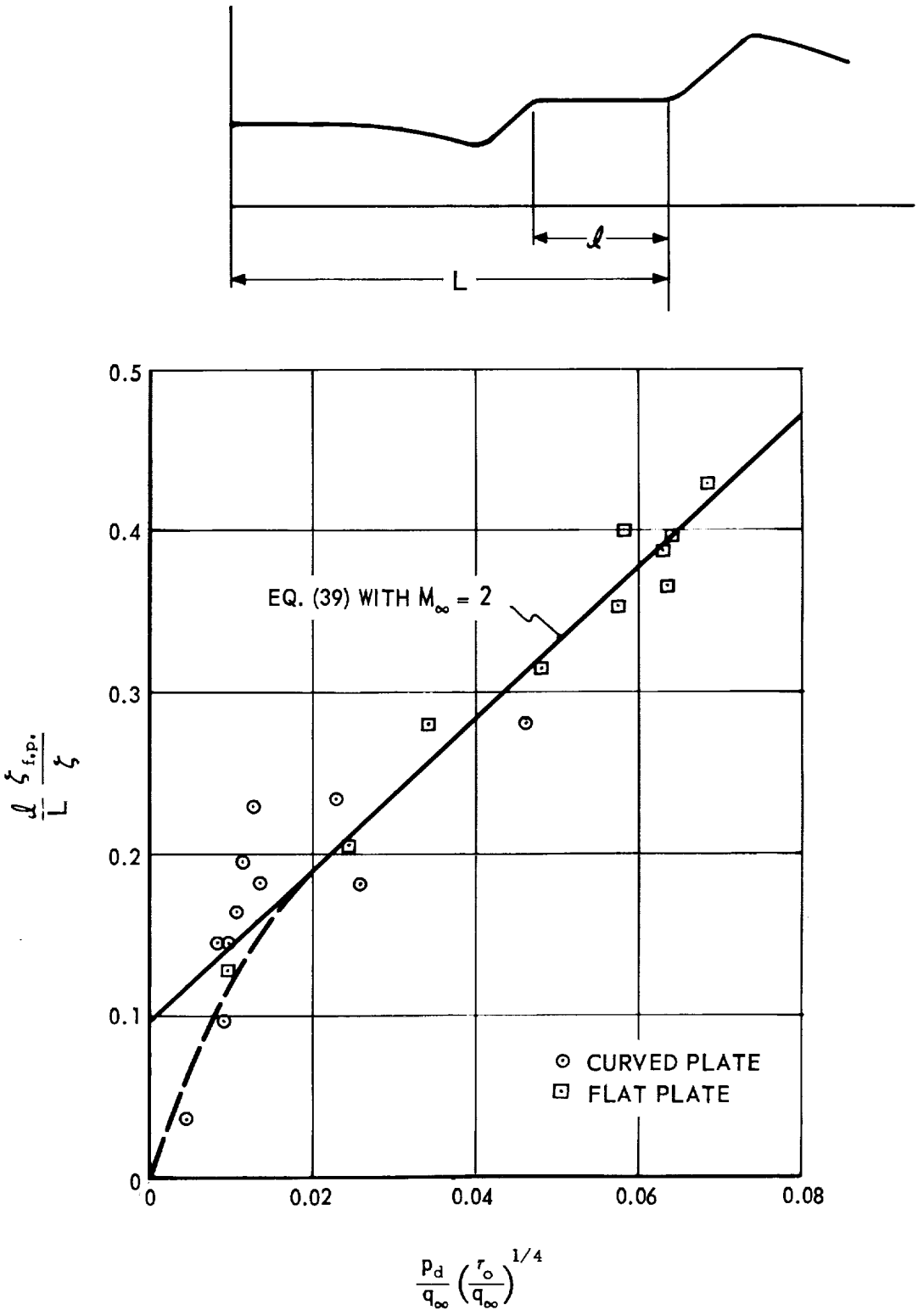

Fig. 8. Length of plateau.

$\frac{R_{\infty}}{ft} \times 10^{-6}$ / x (in.)	0.72	1.04	1.40	1.81	2.16	2.49	3.14	3.24	3.68
0.4	1.103	1.055	1.042	1.034	1.029	1.029	1.028	1.017	1.015
0.5	1.000	1.008	1.000	0.995	1.000	0.993	0.991	0.989	0.990
0.6	1.000	0.991	1.006	1.004	1.010	1.003	1.002	1.005	1.004
0.7	1.000	1.000	1.000	1.000	1.007	1.000	1.000	1.000	1.000
0.8	1.000	1.008	1.006	1.000	1.003	1.003	1.004	1.007	1.004
0.9	1.012	1.008	1.006	1.004	1.007	1.003	1.004	1.005	1.007
1.0	0.991	1.000	0.993	0.990	0.996	0.993	0.994	0.994	0.995
1.1	1.000	1.000	0.993	0.990	0.996	0.996	0.997	0.997	0.997
1.2	0.991	0.991	0.981	0.985	0.988	0.982	0.985	0.984	0.985
1.3	1.000	1.000	0.981	0.985	0.988	0.986	0.988	0.986	0.988
1.4	0.978	0.974	0.969	0.971	0.977	0.976	0.976	0.976	0.976
1.5	1.000	0.991	0.981	0.976	0.984	0.976	0.979	0.979	0.981
1.6	0.978	0.958	0.951	0.948	0.957	0.955	0.955	0.953	0.953
1.7	0.978	0.958	0.951	0.948	0.950	0.949	0.947	0.945	0.946
1.8	0.913	0.916	0.891	0.893	0.897	0.895	0.894	0.896	0.893
1.9	0.900	0.899	0.885	0.888	0.890	0.892	0.889	0.885	0.884
2.0	0.861	0.851	0.836	0.834	0.845	0.837	0.837	0.828	0.833
2.1	0.835	0.835	0.824	0.824	0.830	0.828	0.825	0.820	0.822
2.2	0.809	0.810	0.789	0.787	0.791	0.791	0.790	0.789	0.787
2.3	0.796	0.776	0.771	0.768	0.777	0.773	0.771	0.768	0.769
2.4	0.744	0.734	0.734	0.727	0.739	0.734	0.736	0.735	0.732
2.5	0.722	0.712	0.710	0.704	0.716	0.710	0.710	0.711	0.707
2.6	0.683	0.678	0.675	0.666	0.679	0.673	0.675	0.672	0.670
2.7	0.670	0.662	0.653	0.663	0.664	0.659	0.660	0.656	0.656
2.8	0.683	0.662	0.651	0.644	0.652	0.646	0.646	0.639	0.638
2.9	0.709	0.703	0.687	0.671	0.679	0.673	0.672	0.662	0.658
3.0	0.744	0.726	0.710	0.699	0.706	0.696	0.695	0.686	0.679
3.1	0.770	0.743	0.740	0.732	0.735	0.727	0.727	0.719	0.716
3.2	0.783	0.759	0.746	0.737	0.735	0.730	0.733	0.722	0.718
3.3	0.796	0.776	0.759	0.751	0.754	0.744	0.738	0.735	0.730
3.4	0.796	0.776	0.759	0.746	0.750	0.740	0.738	0.729	0.723
3.5	0.809	0.784	0.771	0.755	0.758	0.747	0.747	0.737	0.730
3.6	0.809	0.784	0.765	0.751	0.754	0.744	0.744	0.735	0.730
3.7	0.822	0.801	0.771	0.763	0.762	0.751	0.747	0.740	0.734

Table I Pressure Distributions (p/p_{∞}) on Curved Plate Without Shock Generator

$\frac{R_{e_\infty}}{ft.} \times 10^{-6}$ / x (in.)	0.99	0.97	1.58	1.57	1.59	1.58	1.75	1.75	1.75
0.4	1.016	1.025	1.005	1.016	1.005	1.010	1.035	1.030	1.020
0.5	1.008	1.000	0.994	1.000	1.000	1.000	1.000	1.000	0.994
0.6	1.000	1.017	1.010	1.016	1.010	1.005	1.010	1.010	1.010
0.7	1.008	1.074	1.000	1.000	1.000	1.000	1.000	1.000	1.000
0.8	1.000	1.126	1.010	1.010	1.005	1.010	1.010	1.010	1.010
0.9	1.008	1.178	1.010	1.010	1.005	1.010	1.010	1.010	1.010
1.0	1.000	1.195	0.994	1.000	0.994	0.994	0.995	0.994	0.994
1.1	1.000	1.212	0.994	1.000	0.994	0.994	1.000	0.994	0.994
1.2	1.000	1.218	0.983	0.989	0.984	0.984	0.985	0.986	0.984
1.3	1.000	1.235	0.983	0.989	0.989	0.994	0.990	0.986	0.984
1.4	0.984	1.218	0.973	0.978	0.994	1.021	0.971	0.976	0.969
1.5	0.984	1.235	0.973	0.978	1.026	1.051	0.975	0.976	0.974
1.6	0.962	1.235	0.946	0.967	1.067	1.099	0.951	0.951	0.974
1.7	0.954	1.244	0.941	0.994	1.099	1.115	0.946	0.941	1.010
1.8	0.946	1.235	0.905	1.032	1.108	1.129	0.896	0.901	1.058
1.9	0.992	1.235	0.946	1.078	1.139	1.156	0.926	0.956	1.093
2.0	1.008	1.226	0.962	1.078	1.125	1.134	0.911	0.976	1.088
2.1	1.000	1.226	1.000	1.078	1.125	1.134	0.966	1.010	1.098
2.2	0.992	1.235	1.005	1.078	1.125	1.134	0.985	1.015	1.098
2.3	0.938	1.244	1.062	1.115	1.134	1.145	1.030	1.075	1.118
2.4	0.914	1.244	1.067	1.142	1.171	1.182	1.020	1.093	1.146
2.5	0.882	1.278	1.056	1.221	1.286	1.314	0.990	1.103	1.250
2.6	0.882	1.287	1.040	1.221	1.313	1.339	0.961	1.087	1.255
2.7	0.930	1.312	1.035	1.215	1.334	1.376	0.956	1.075	1.270
2.8	0.946	1.330	1.040	1.204	1.313	1.349	0.961	1.065	1.250
2.9	0.976	1.347	1.062	1.210	1.323	1.365	1.020	1.108	1.250
3.0	0.984	1.372	1.094	1.183	1.292	1.344	1.025	1.113	1.222
3.1	0.992	1.381	1.126	1.256	1.318	1.355	1.050	1.159	1.255
3.2	0.992	1.395	1.126	1.231	1.302	1.349	1.050	1.164	1.237
3.3	0.992	1.404	1.131	1.304	1.369	1.397	1.065	1.179	1.338
3.4	0.984	1.413	1.131	1.288	1.423	1.470	1.060	1.179	1.325
3.5	0.992	1.421	1.137	1.326	1.479	1.548	1.070	1.184	1.383
3.6	0.992	1.456	1.131	1.372	1.605	1.669	1.060	1.174	1.487
3.7	0.992	1.464	1.137	1.372	1.647	1.744	1.070	1.192	1.489

Note: Runs grouped by a brace (⌣) represent approximately a constant free stream Reynolds number with varying shock strength.

Table II - Pressure Distributions (p/p_∞) on Curved Plate With Impinging Shock

$\frac{R_{e_\infty}}{ft.} \times 10^{-6}$ / x (IN.)	1.75	1.92	1.90	1.86	1.84	2.18	2.15	2.14	2.28
0.4	1.020	1.021	1.021	1.296	1.022	1.015	1.011	1.007	1.014
0.5	0.994	1.000	0.995	1.000	0.990	0.988	0.992	0.988	0.992
0.6	1.005	1.009	1.009	1.009	1.004	1.003	1.000	1.000	1.003
0.7	1.000	1.000	1.000	1.014	1.000	1.000	0.996	0.992	1.000
0.8	1.005	1.004	1.004	1.009	1.000	1.000	1.000	1.000	1.000
0.9	1.005	1.004	1.004	1.009	1.004	1.000	1.000	0.996	1.000
1.0	0.994	0.990	0.990	0.995	0.990	0.984	0.988	0.984	0.989
1.1	0.994	0.995	0.990	1.000	0.990	0.988	0.988	0.984	0.989
1.2	0.984	0.981	0.976	0.985	0.980	0.977	0.978	0.972	0.981
1.3	0.994	0.981	0.981	0.985	0.980	0.977	0.978	0.976	0.981
1.4	1.030	0.968	0.963	0.976	0.985	0.966	0.970	0.964	0.975
1.5	1.078	0.972	0.967	0.976	1.014	0.966	0.970	0.964	0.975
1.6	1.119	0.949	0.944	0.962	1.060	0.943	0.943	0.942	0.954
1.7	1.134	0.949	0.944	0.985	1.088	0.940	0.939	0.938	0.954
1.8	1.147	0.901	0.909	1.023	1.111	0.888	0.890	0.895	0.904
1.9	1.172	0.919	0.930	1.050	1.115	0.899	0.890	0.923	0.925
2.0	1.152	0.924	0.963	1.069	1.115	0.906	0.905	0.960	0.939
2.1	1.157	0.963	1.000	1.074	1.115	0.951	0.958	0.996	0.954
2.2	1.152	0.936	1.013	1.078	1.120	0.920	0.978	1.000	0.917
2.3	1.167	0.896	1.067	1.116	1.139	0.883	0.996	1.023	0.882
2.4	1.213	0.860	1.081	1.147	1.182	0.845	0.974	1.076	0.842
2.5	1.395	0.820	1.067	1.222	1.317	0.804	0.939	1.072	0.804
2.6	1.444	0.788	1.041	1.213	1.326	0.770	0.908	1.045	0.778
2.7	1.505	0.784	1.021	1.208	1.346	0.748	0.878	1.019	0.764
2.8	1.500	0.806	1.016	1.180	1.317	0.755	0.875	1.003	0.775
2.9	1.510	0.855	1.058	1.185	1.326	0.808	0.920	1.019	0.822
3.0	1.479	0.864	1.067	1.156	1.307	0.816	0.931	1.053	0.833
3.1	1.474	0.873	1.107	1.213	1.312	0.834	0.966	1.080	0.846
3.2	1.454	0.878	1.107	1.180	1.303	0.834	0.966	1.084	0.846
3.3	1.474	0.882	1.118	1.268	1.341	0.845	0.974	1.104	0.846
3.4	1.568	0.878	1.121	1.244	1.388	0.841	0.974	1.100	0.846
3.5	1.697	0.882	1.130	1.301	1.490	0.845	0.978	1.114	0.846
3.6	1.771	0.878	1.118	1.356	1.566	0.845	0.978	1.107	0.853
3.7	1.890	0.887	1.139	1.361	1.655	0.849	0.984	1.126	0.857

Table II - Pressure Distributions (p/p_∞) on Curved Plate With Impinging Shock

(Continued)

$\frac{R_{e_{ft.}}}{ft.} \times 10^{-6}$ / x (IN.)	2.19	2.16	2.13	2.73	2.76	2.73	2.73	2.57	2.56
0.4	1.013	1.019	1.015	1.018	1.015	1.017	1.019	1.015	1.019
0.5	0.992	0.993	0.988	0.990	0.991	0.993	0.993	0.993	0.990
0.6	1.000	1.003	1.004	1.003	1.003	1.005	1.006	1.003	1.003
0.7	1.000	1.003	1.000	1.000	1.000	1.000	1.000	1.000	1.000
0.8	1.003	1.000	1.000	1.006	1.003	1.005	1.006	1.003	1.003
0.9	1.003	1.000	1.000	1.006	1.003	1.003	1.006	1.003	1.003
1.0	0.988	0.989	0.988	0.996	0.993	0.990	0.996	0.990	0.990
1.1	0.992	0.993	0.996	0.996	0.993	0.993	0.996	0.993	0.993
1.2	0.981	0.985	1.039	0.984	0.982	0.984	0.984	0.983	0.981
1.3	0.981	0.989	1.076	0.984	0.985	0.984	0.978	0.983	0.981
1.4	0.969	1.011	1.125	0.972	0.969	0.974	0.975	0.970	0.971
1.5	0.981	1.057	1.137	0.972	0.969	0.974	0.978	0.973	0.971
1.6	0.981	1.095	1.152	0.952	0.947	0.952	0.978	0.950	0.948
1.7	1.013	1.114	1.152	0.934	0.944	0.955	1.015	0.947	0.944
1.8	1.058	1.126	1.156	0.895	0.895	0.981	1.059	0.892	0.902
1.9	1.074	1.133	1.156	0.895	0.911	1.008	1.075	0.895	0.919
2.0	1.077	1.133	1.156	0.892	0.941	1.036	1.078	0.889	0.957
2.1	1.084	1.133	1.156	0.952	0.982	1.043	1.085	0.889	0.990
2.2	1.080	1.133	1.179	0.963	1.018	1.043	1.078	0.967	0.996
2.3	1.132	1.194	1.419	0.955	1.050	1.080	1.104	0.963	1.055
2.4	1.176	1.303	1.708	0.925	1.058	1.124	1.157	0.932	1.075
2.5	1.265	1.482	1.849	0.883	1.043	1.204	1.298	0.892	1.075
2.6	1.265	1.531	1.761	0.850	1.018	1.195	1.310	0.860	1.055
2.7	1.243	1.517	1.777	0.821	0.985	1.167	1.298	0.834	1.019
2.8	1.218	1.463	1.670	0.815	0.966	1.151	1.292	0.834	1.006
2.9	1.207	1.474	1.681	0.850	0.972	1.132	1.267	0.882	1.016
3.0	1.176	1.429	1.658	0.865	0.979	1.111	1.251	0.892	1.017
3.1	1.191	1.414	1.625	0.895	1.037	1.132	1.251	0.922	1.075
3.2	1.173	1.391	1.613	0.898	1.037	1.102	1.238	0.922	1.078
3.3	1.235	1.414	1.697	0.907	1.064	1.198	1.257	0.932	1.105
3.4	1.250	1.471	1.753	0.904	1.058	1.186	1.301	0.928	1.101
3.5	1.332	1.619	1.880	0.910	1.074	1.248	1.412	0.932	1.115
3.6	1.444	1.691	2.042	0.910	1.067	1.335	1.489	0.932	1.111
3.7	1.476	1.797	2.126	0.916	1.086	1.348	1.584	0.935	1.133

Table II - Pressure Distributions (p/p_∞) on Curved Plate with Impinging Shock

(Continued)

$\frac{R_{ft}}{ft.} \times 10^{-6}$ / x (IN.)	2.61	3.75	3.74	3.60	3.59	3.57	3.58
0.4	1.013	1.022	1.015	1.020	1.013	1.013	1.020
0.5	0.993	0.999	0.993	1.000	0.993	0.994	1.000
0.6	1.009	1.017	1.006	1.013	1.009	1.008	1.015
0.7	1.000	1.006	1.000	1.006	1.000	1.000	1.004
0.8	1.009	1.000	1.008	1.016	1.006	1.008	1.013
0.9	1.009	1.017	1.010	1.013	1.009	1.008	1.015
1.0	0.993	1.001	0.993	1.000	0.993	0.993	1.000
1.1	0.996	1.003	0.995	0.979	0.993	0.997	1.001
1.2	0.983	0.990	0.981	0.987	0.981	0.981	0.985
1.3	0.983	0.992	0.984	0.993	0.983	0.983	0.988
1.4	0.973	0.981	0.972	0.982	0.969	0.974	0.978
1.5	0.973	0.979	0.972	0.979	0.969	0.971	0.978
1.6	0.958	0.959	0.950	0.958	0.949	0.951	0.958
1.7	0.970	0.949	0.943	0.951	0.942	0.946	0.963
1.8	0.986	0.889	0.885	0.892	0.887	0.916	0.981
1.9	1.038	0.905	0.908	0.913	0.903	0.955	1.020
2.0	1.054	0.887	0.934	0.901	0.920	0.994	1.039
2.1	1.064	0.952	0.970	0.951	0.961	1.008	1.046
2.2	1.060	0.947	0.972	0.910	0.965	1.008	1.041
2.3	1.083	0.923	1.035	0.862	1.031	1.050	1.066
2.4	1.125	0.885	1.062	0.821	1.048	1.100	1.129
2.5	1.230	0.838	1.066	0.775	1.029	1.153	1.238
2.6	1.233	0.811	1.044	0.746	1.006	1.139	1.234
2.7	1.220	0.777	1.006	0.714	0.969	1.105	1.203
2.8	1.205	0.768	0.995	0.718	0.958	1.093	1.194
2.9	1.189	0.784	0.979	0.739	0.951	1.068	1.166
3.0	1.163	0.802	0.977	0.766	0.951	1.057	1.154
3.1	1.182	0.840	1.028	0.782	1.011	1.082	1.154
3.2	1.151	0.845	1.028	0.794	1.013	1.064	1.139
3.3	1.236	0.853	1.068	0.791	1.041	1.142	1.196
3.4	1.246	0.853	1.066	0.801	1.038	1.138	1.235
3.5	1.307	0.855	1.087	0.794	1.048	1.184	1.286
3.6	1.416	0.860	1.096	0.805	1.057	1.230	1.379
3.7	1.439	0.862	1.118	0.805	1.068	1.253	1.432

Table II - Pressure Distributions (p/p_∞) on Curved Plate with Impinging Shock

(Concluded)